JOURNAL OF APPLIED ELECTROCHEMISTRY **28** (1998) 979–992

Determination of the oxygen reduction products on ASTM A516 steel during cathodic protection

D. GERVASIO[†,1], I. SONG[*,2] J. H. PAYER[2]

Ernest Yeager Center for Electrochemical Sciences,[1] and Department of Materials Science and Engineering,[2] The Case School of Engineering Case Western Reserve University, Cleveland, OH 44106, USA

Received 25 June 1997; revised 15 January 1998

The electrochemistry of steel in aerobic and anaerobic aqueous alkaline solutions was studied with or without forced convection to investigate the cathodic processes occurring on steel exposed by defects in polymer coated steel pipe. The results are relevant to the mechanistic understanding of the effect of cathodic protection on the disbonding of fusion bonded epoxy (FBE) coatings on steel. Moderate (pH 9.8) and strongly (pH 14) alkaline aqueous solutions were used to simulate the water layers at the cathodically polarized steel surface on the soil-side of buried pipe. A rotating gold ring and steel disc electrode (RRDE) in alkaline aqueous electrolyte equilibrated with 1 atm oxygen over solution was used to measure the rotation rate dependent current for the electroreduction of oxygen, O_2, on an ASTM A516 steel disc and the resulting peroxide generation, which was determined by monitoring the oxidation current on the gold ring. An appreciable fraction of the oxygen reduction current on the steel disk gave rise to peroxide generation over a wide range of potentials, from −0.2 to −0.9 V vs SCE in 1 M KOH. The observation of peroxide generation is noteworthy, because oxidizing agents, such as peroxide and its decomposition products, superoxide and hydroxy radical, can degrade the polymers used for coating pipelines. As result, oxidative degradation of polymer or interfacial compounds may be a cause of the accelerated disbonding observed for protective coatings on steel pipelines under cathodic protection.

Keywords: *oxygen reduction*, *steel*, *cathodic protection*, *peroxide production*, *polymer degradation*

1. Introduction

Steel corrosion in soil is due to the electrochemical oxidation of the metal at anodic sites coupled to the reduction of oxygen at cathodic sites. The corrosion current and cathodic current densities are strongly dependent on the oxygen electroreduction process. There have been only a few electrochemical studies reported for the electroreduction of oxygen on iron and steel [1–3]. The objective of this research was to determine the cathodic reactions on steel in air-saturated water. The results are relevant to the understanding of the effect of cathodic protection on the disbonding of coatings on buried pipelines.

Typically, the exterior of buried steel pipe in soil is protected from corrosion by an electrically insulating organic coating and by cathodically protecting any steel that may be exposed at defects in the coating. Disbonding of the protective coatings is reported to occur faster when cathodic protection is applied than when there is no cathodic protection [4]. This accelerated disbonding has often been suspected of being a phenomenon that may, at least in part, be due to a chemical attack of the coating by peroxide (and/or its decomposition products, namely, superoxide and hydroxy radical) formed as an intermediate during the electroreduction of oxygen on the cathodically polarized steel surface [2, 3]. In addition, the peroxide, superoxide and hydroxy radial may have significant effects on interfacial compounds. A first rational step to test this chemical attack hypothesis is to determine if peroxide is forming on pipeline steel under cathodic protection conditions. Consequently, oxygen reduction on steel was investigated to determine the chemical species produced on a steel surface in air at various levels of cathodic protection. Additional efforts have been made from other technical perspectives to determine if the oxygen reduction products can degrade the protective coatings and contribute to the disbonding of the coating from the steel surface [5].

A rotating gold ring and steel disc electrode (RRDE) was used to study oxygen reduction on steel. In the RRDE technique the species of interest in bulk solution is convected to the disc electrode and then flows away from the disc to the ring electrode. The steel disc potential was slowly swept through the

[*] The author to whom correspondence should be addressed. Present address: IMQ Corporation, PO Box 241026, Cleveland, OH 44124, USA
[†] Note: D. Gervasio is now with Mail Stop EL 703, Motorola, Phoenix Corporate Research Laboratory, 2100 East Elliott Road, Temple, Arizona 85284, USA

0021-891X

oxygen reduction region, and as peroxide formed on the steel disc and was liberated into solution, it was detected on the gold ring, which was poised at a potential for peroxide oxidation. The greater the rotation rate, the greater the mass transfer of oxygen from bulk solution to the disc and oxygen reduction products from the disc to the ring. The RRDE technique results in greater faradaic currents at higher rotation rates, and therefore greater sensitivity of the ring to peroxide formed at the disc, provided there is no deactivation of the gold ring due to the excessive transport of inhibitors (i.e., species that alter the characteristics of the ring electrode to peroxide electrooxidation) to the gold surface.

2. Background for oxygen reduction on steel

Table 1 summarizes the chemistry of molecular oxygen, O_2, pertinent to the electroreduction of oxygen in alkaline (pH 14) media and gives the potentials and energies for the chemical reactions. The data in Table 1 suggest that the electroreduction of molecular oxygen should directly produce hydroxide, OH^-, via a four-electron process starting at $+0.159$ V vs SCE and at more negative potentials. This is not the observed behaviour on steel in aqueous alkaline solution. Instead, the reduction of oxygen on steel in alkaline solution leads first to the formation of peroxide, and this does not begin until -0.3 V vs SCE. The reason for this apparent paradox is that the data in Table 1 give the thermodynamic potentials separating the oxidation states but not the kinetic barriers to these transformations. Although the four-electron reduction of O_2 on steel in alkaline water is more favoured thermodynamically than the two-electron reduction, the kinetic barrier for the four-electron pathway is greater than for the two-electron pathway.

The set of specific kinetic factors for oxygen reduction on steel (i.e., the mechanism of O_2 electroreduction on steel in alkaline water solutions) has received little attention [1–3]. There has been considerable attention given to oxygen reduction for fuel cell applications and for metal/air battery systems. The general mechanism for oxygen electroreduction is fairly well understood and has been reviewed in the literature [1, 7, 8]. Although oxygen is just a homonuclear diatomic molecule, oxygen electrochemistry is complex owing to its complex electronic structure, that is, relative to the simple electronic structure and electrochemistry of homonuclear diatomic hydrogen. The pertinent electronic structure of oxygen is represented by the molecular orbital (MO) diagram of the valence orbitals of molecular oxygen. The molecular orbitals can be considered to be linear combinations of the 2s and 2p orbitals from two oxygen atoms, each of which contributes six valence electrons [9]. The 2s orbitals result in a closed shell, that is, the completely filled σ^b2s and σ^a2s orbitals (not shown). The molecular orbitals formed from the 2p valence orbitals are shown in Fig. 1.

Molecular oxygen can be completely reduced to two oxide dianion species (the water oxidation state) by accepting four electrons. An electrode can be the source of electrons, and molecular oxygen dissolved in water the sink of electrons. The higher the overpotential of the electrode, the more the electrode is able to put electrons into the empty higher energy molecular orbitals of O_2. The MO diagram of O_2 in Fig. 1 shows that the lowest energy empty orbitals available for accepting electrons are the two half filled, equal π^a2p orbitals. Completing the occupancy of these orbitals with two electrons converts molecular oxygen to the diatomic peroxide oxidation state. Peroxide is usually formed at low overpotentials (low electronic energies) on steel and on many other metal electrodes which have poor catalytic surfaces for oxygen reduction [10–12]. For O_2 reduction on steel in 1 M KOH, this low overpotential region is between around -0.3 and -0.8 V vs SCE [1, 13]. Further reduction can only occur by populating the higher energy σ^a2p orbital. Adding two more electrons to the σ^a2p orbital results in the breaking of the O–O

Table 1. Reduction potentials of O_2 and related species at pH14 [6]

Reaction	E_b^o /V vs NHE	E_b^o /V vs SCE
Hydroxide, OH^-		
$O_2 + 2H_2O + 4e^- \rightarrow 4OH^-$	0.401	(0.159)
Peroxide, H_2O_2		
$O_2 + H_2O + 2e^- \rightarrow HO_2^- + OH^-$	−0.076	(−0.318)
$HO_2^- + H_2O + 2e^- \rightarrow 3OH^-$	0.87	(0.628)
$Na_2O_2 + 2H_2O + 2e^- \rightarrow 4OH^- + 2Na^+$	1.23	(0.988)
$2HO_2^- \rightarrow 2OH^- + O_2$	$\Delta G° = -43\,950$ calories	
Superoxide, $^*O_2H$		
$O_2 + e^- \rightarrow {}^*O_2^-$	−0.6	(−0.842)
$^*O_2^- + H_2O + e^- \rightarrow HO_2^- + OH^-$	0.4	(0.158)
$2{}^*O_2H \rightarrow H_2O_2 + O_2$	$\Delta G° = -37\,500$ calories	
$^*O_2^- + 2H_2O + 3e^- \rightarrow 4OH^-$	0.7	(0.458)
Hydroxy radical, $^*OH$		
$1/2\,O_2 + H_2O + e^- \rightarrow {}^*OH + OH^-$	−0.61	(−0.852)
$^*OH + e^- \rightarrow OH^-$	1.4	(1.15)

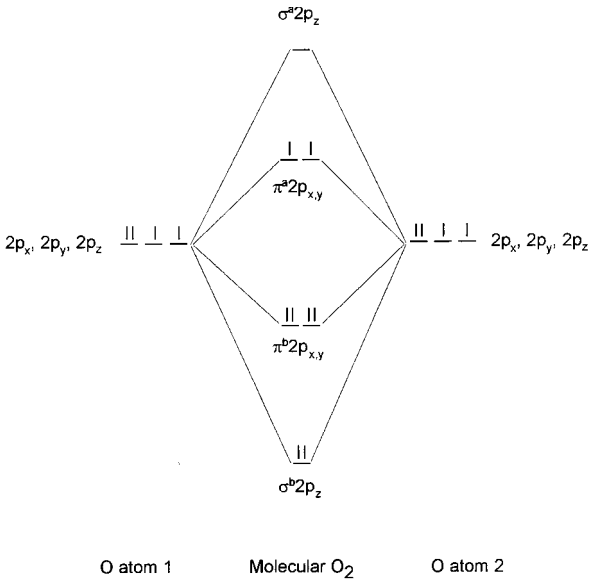

Fig. 1. Molecular orbitals of diatomic oxygen, O_2, from oxygen atomic orbitals.

bond and the conversion of peroxide to two hydroxide species. This occurs at high overpotentials (high excess electronic energies). For ASTM A516 steel in 1 M KOH, this high overpotential region is found at in the range from −0.9 to −1.2 V and more negative potentials vs SCE. The difference in energy between the π^a2p orbitals and the σ^a2p orbital is approximately the electronic contribution to the difference in energy between the barriers to the two-electron versus four-electron pathways.

The direct four-electron transfer from steel to oxygen (O_2) can only occur if some portion of the electrode surface has a stabilizing (bonding) interaction with the σ^a2p orbital, so that the σ^a2p orbital is lowered in energy to the level of the π^a2p orbitals. Four electron reduction of O_2 on platinum is explained this way [7]. It has been suggested that at high overpotentials, the surface of an iron electrode is fully reduced, and that the metallic iron electrode promotes the direct four-electron reduction of O_2 to OH^- is neutral and mildly alkaline water solutions [1]. It is more likely, however, that oxygen reduction occurs by first filling the π^a2p orbital with two electrons and then filling the σ^a2p orbital with two electrons to give OH^-, as explained above. At high overpotentials, it may be impossible to distinguish a direct four-electron reduction from a pair of two-electron reduction steps, because, either way, so little peroxide escapes into solution, that peroxide detection, the distinguishing factor, is not practically possible.

The mechanism of oxygen reduction can be rationalized from a phenomenological standpoint. At any given electrode potential, the electroreduction of oxygen may occur by two pathways: (i) a direct four electron reduction of O_2 to give the endproduct, water, at a rate linearly dependent on O_2 concentration and specified by the rate constant k_1; and (ii) a two step series process. The first step is the two electron reduction of oxygen to give peroxide in a first order process with rate constant, k_2. The second step is the two electron reduction of peroxide to give water in a first order process with rate constant, k_3. Peroxide may escape into solution during the series pathway but not during the direct four-electron pathway. With the series pathway operative, the peroxide may, therefore, undergo a chemical decomposition instead of undergoing the second two electron reduction. This is summarized by the simplified general mechanism for the electroreduction of oxygen shown in Fig. 2 [2, 7].

At a particular electrode potential, both the direct pathway and the series pathway may occur simultaneously on different parts of the steel electrode surface, and in this case of the O_2 reduction is said to occur by a parallel pathway. The first RRDE study of O_2 reduction on iron in neutral and mildly alkaline water reported that at low overpotentials on passivated iron, the two-electron reduction of O_2 occurs to give H_2O_2 as the endproduct via the series mechanism; and at high overpotentials on metallic iron, principally the four-electron reduction product, water, forms via the direct or parallel pathway [1]. Later, the electroreduction of O_2 was reported to produce mainly peroxide at low overpotentials, and hydroxide at high overpotentials via the series pathway (i.e., by two sequential two-electron steps) at all potentials for low carbon steel in aqueous 1 M NaOH solution [3]. Others report that for pure iron in pH 9.8 buffer, O_2 reduction proceeds by the series pathway in the low overpotential region, but that since very little peroxide is generated at higher overpotentials, it is probably not possible to make a reliable distinction between the parallel and series mechanism [2].

There is general agreement that as O_2 is electroreduced on the prepassive and passive steel surface (E_{steel} = −0.2 to −0.9 V vs SCE for 1 M KOH) in alkaline water, large amounts of peroxide are continuously being generated. A large concentration of peroxide rapidly builds up near the surface. The prepassive and passive surfaces are covered by Fe^{2+} and Fe^{3+} species. Table 2 lists the possible reactions between peroxide and the ferrous and ferric ions [14], and these represent the situations expected to be found on the cathodically protected steel surface.

Having peroxide and iron ions on the surface would present a situation ideal for the iron–ion-catalysed disproportionation of peroxide to oxy radicals previously; however, it was reported that for O_2 re-

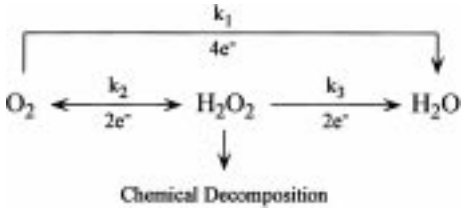

Fig. 2. Pathways for electroreduction of oxygen. k_1: rate constant for direct $4e^-$ reduction of O_2 to water; k_2: rate constant for $2e^-$ reduction of O_2 to peroxide; and k_3: rate constant for $2e^-$ reduction of peroxide to hydroxide.

Table 2. Possible interactions between peroxide, and the ferrous and ferric ions

$Fe^{2+} + H_2O_2 \rightarrow Fe^{3+} + {}^{*}OH + OH^{-}$
$Fe^{2+} + {}^{*}OH \rightarrow Fe^{3+} + OH^{-}$
$H_2O_2 + {}^{*}OH \rightarrow {}^{*}O_2H + H_2O$
$Fe^{2+} + {}^{*}O_2H \rightarrow Fe^{3+} + HO_2^{-}$
$Fe^{3+} + {}^{*}O_2H \rightarrow Fe^{2+} + H^{+} + O_2$

duction studied by the RRDE method, there was no indication that catalytic decomposition of peroxide occurred [2, 3]. The iron-ion catalysed disproportionation kinetics may be slow relative to the peroxide generation arising from the O_2 reduction on the same surface. In this case, much peroxide would escape into solution before it was chemically decomposed to radicals by the catalytic action of iron ions on the surface. As a result, peroxide decomposition would be difficult to observe electrochemically, because the disproportionation of peroxide to radicals would account for a lowering of the peroxide oxidation current on the gold ring by less than a few percent. A small percentage change is not readily detected by the RRDE method. Nevertheless, although it is uncertain whether a small percentage of the peroxide is being converted to because the radical species are typically more reactive and degrading than peroxide itself, the long term cumulative effect of such radicals on the coating itself or on the integrity of the coating/steel interface should be considered as an additional possible source of degradation of the FBE coated steel pipeline.

3. Experimental details

Electrolyte solutions were made with ultrapure water prepared by reverse osmosis and distillation. Potassium hydroxide stock was Fisher 45 wt. % 'Certified Reagent' grade. Sodium borate decahydrate was in powder form, Mallinckrodt, Analytical Reagent grade. Nitrogen and oxygen were Linde dry grade purified by passing the gas through a 0.4 nm (~4 Å) molecular sieve. All gases were presaturated with water by passing the purified gas through ultrapure water in a gas wash bottle. Peroxide was Hach 50% aqueous solution with no stabilizer. The pH of solutions was measured with an Orion pH meter using a glass electrode. Electrochemical measurements were carried out at room temperature in a three compartment Pyrex cell. A gold counter electrode was used. The reference compartment was connected to the main compartment via a Luggin capillary. Either a saturated calomel electrode (SCE, $E = +242$ mV vs NHE) or a reversible hydrogen electrode (RHE, related to NHE by the pH difference times 59 mV decades^{-1} of pH) was the reference electrode. Gold electrodes were prepared for voltammetry experiments by heating in a gas/air flame and plunging into ultrapure water while still red hot. The RRDE was Pine model AFMTI34DC Au T electrode which is equipped with a gold ring (i.d. 0.75 cm; o.d 0.85 cm) with a transferable disc capability ($d = 0.608$ cm). In this study, an ASTM A516 steel disc was used for oxygen reduction studies. The elemental analysis of the steel showed that the steel consists of 1% Mn, 0.2% C and 0.2% Si and the balance is Fe (the analysis done by Herron Testing Laboratories, Cleveland, OH). A polycrystalline gold (+99.999%, Pine) disc was used for electrode geometry calibration studies. After assembly, the RRDE was prepared by lightly lapping with 1200 SiC paper, and then polishing with successively finer grades of alumina (15, 10, 5, 1, 0.3 and 0.05 μm). The electrode was buffed with 0.05 μm alumina and rinsed with ultrapure water before each measurement. The working electrode potential was controlled using a potentiostat (model BC-1200, Stonehart) connected to a waveform generator (model 175, PAR). RRDE experiments were controlled by using two BC-1200 potentiostats in the inverted configuration, that is, with the counter electrode being the electrical ground. Rotation of the RRDE was done with a Pine AFMSRX rotator controlled by a Pine MSRX speed controller. The current response was recorded on a set of X–Y recorders (Watanabe WX1000 and PAR RE0074). The collection efficiency of the ring was experimentally determined to be 0.24 using the reduction of 0.005 molar ferricyanide in borate buffer (pH 9.8) [15]. This was in good agreement with the theoretically expected value of 0.23 based on the disc- and ring-electrode geometry [16]. Oxygen reduction measurements were quasi-steady state, because in these experiments the RRDE disc was slowly scanned. The gold ring was first activated by cycling it through the gold oxide formation and reduction region and then was held at a constant potential vs SCE during peroxide detection.

4. Results

4.1. *Voltammetry experiments*

The voltammetry of steel was done in alkaline aqueous solution to determine the electrochemical processes that may occur on the moisture covered steel surface and the potentials associated with these processes. The typical ground waters vary in pH; however, the water in contact with steel becomes more alkaline as a result of cathodic protection [17]. Aqueous alkaline potassium hydroxide (pH 14) and borate buffer (pH 9.8) solutions were studied to examine a strongly and a mildly alkaline environment. Voltammetry performed under an inert (N_2) atmosphere was useful for checking the condition of the interface before the RRDE measurements.

Gold and platinum are well behaved, losing their nascent oxide on the first cathodic scan and achieving their steady state surface on the second cycling of potential. The amount of oxide that formed in the subsequent anodic scan depended only on scan rate and the potential. Iron and steel, however, being

more active metal, required holding the electrode near the hydrogen evolution potential (~−0.27 V vs RHE or ~−1.35 V vs SCE for 1 M KOH, pH 14) for about 10 min for the removal of the nascent oxide formed during mechanical polishing and preparation. This behaviour has been recently reviewed and spectroscopically confirmed for iron [18, and the references cited therein] and is attributed to a net accumulation of iron oxide per cycle. ASTM A516 steel exhibits electrochemical behavior similar to low carbon steels and pure iron.

The cyclic voltammogram of gold in anaerobic and aerobic solutions of aqueous 1 M KOH are shown in Fig. 3. Curve (a) is characteristic of a clean gold surface, and this indicates that this electrolyte solution was fairly pure. Curve (b) shows the change in the gold voltammogram when this system is equilibrated with 1 atm of oxygen over solution. The most noticeable difference between the anaerobic and aerobic solutions is the cathodic current for oxygen reduction which onsets at −0.2 V vs SCE and continues to the hydrogen evolution potential at −1.35 V. Oxygen reduction on gold in aqueous alkaline media results in peroxide formation until high cathodic overpotentials where hydroxide forms [19]. The inflection in the current response at −0.8 V vs SCE in Fig. 3, Curve (b) probably marks the onset of this high overpotential region. During the return scan in the positive direction, an excess oxidation current can be seen beginning at around −0.25 V vs SCE and continuing to more positive potentials. The excess oxidation current is due to peroxide eletrooxidation. The peroxide that is being oxidized remained in the diffusion layer after it formed during oxygen reduction on the gold surface in the quiescent solution. The oxidation wave peaks at around −0.2 V vs SCE and is diffusion limited at +0.05 V vs SCE, as is evidenced by the downward sloping of the wave at this potential.

Although platinum is a more active peroxide oxidation electrode than gold, there may be some problem using an anodically biased platinum ring as an electrode for detecting oxygen reduction products formed on a cathodically biased steel disc. This has been mentioned by others [2, 3]. Apparently the problem arises from contamination of the steel disc by the platinum ring. This occurs either during the mechanical polishing or during the electrochemical measurements due to dissolution of platinum at the anodic ring potential. The contamination of the disc by platinum may arise during electrochemical measurements, because with the platinum ring at a relatively positive, peroxide oxidizing potential and the steel disc at a relatively negative, oxygen reducing potential, the platinum could electroplate onto the steel disc. Regardless of how the platinum contamination of the disc occurs, platinum is a very active O_2 reduction catalyst, and trace platinum on a steel substrate would dominate the oxygen reduction catalysis [20], and possibly invalidate the experiments. Gold is a much less active oxygen reduction catalyst and a more noble metal under the conditions of this study. Gold was found to be a suitable electrode for detecting peroxide by peroxide oxidation, because transport limited peroxide oxidation occurs on gold, and it occurs at potentials cathodic of gold oxide formation (Fig. 3). Therefore, gold is better suited than platinum and was selected as the material for the detector electrode of the peroxide formed on the cathodically biased steel.

The voltammetry for the ASTM A516 steel disc in anaerobic aqueous 1 M potassium hydroxide is shown in Fig. 4. The potential window for this measurement is limited by hydrogen evolution at about −1.35 V vs SCE and oxygen evolution at about +0.55 V vs SCE. The electrode was freshly polished with 0.05 μm alumina, the final grit size during electrode preparation. The polished electrode was then stirred in the anaerobic 1 M KOH solution by rotating at 1600 rpm for a few minutes. The open circuit potential converged on −520 mV vs SCE. The initial potential for the first scan was −520 mV and the initial scan

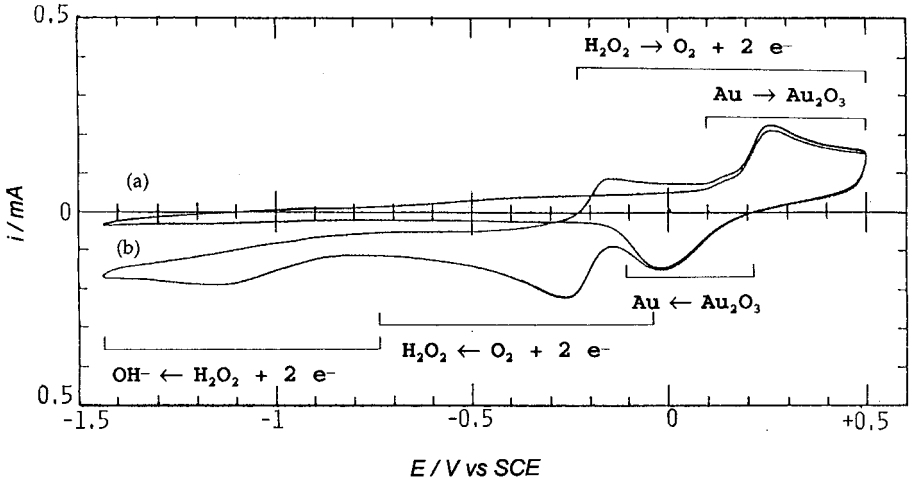

Fig. 3. Cyclic voltammogram of gold ring (i.d. 0.75 cm, o.d. 0.85 cm) in (a) anaerobic 1 M KOH (pH 14); and (b) equilibrated with 1 atm of oxygen over solution. Scan rate 500 mV s^{-1}.

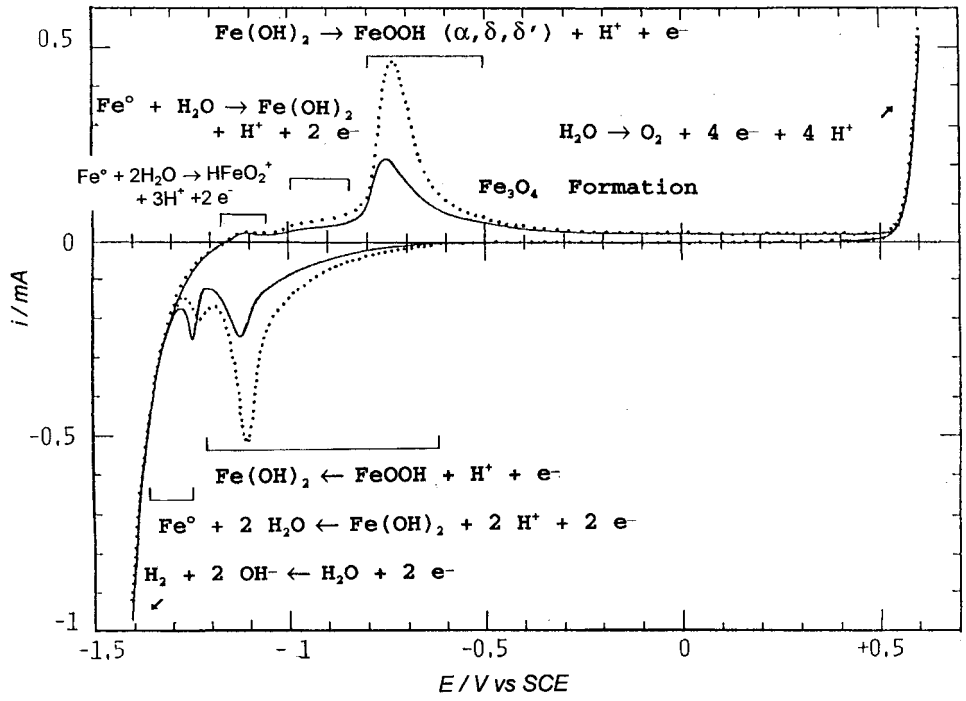

Fig. 4. Cyclic voltammogram of ASTM A516 steel disc (dia. 0.608 cm) in aqueous anaerobic 1 M KOH solution (pH 14). Scan rate 10 mV s^{-1}. Solid line: first curve from the open circuit potential (−520 mV vs SCE) going in the negative direction. Dotted line: the tenth cycle.

direction was toward more negative potentials (see Fig. 4, solid line). Cycling was uninterrupted. All the peaks grew with each cycle and converged on the peak heights shown in the tenth cycle (dotted line in Fig. 4). The voltammograms in Fig. 4 are similar to those reported in a spectroelectrochemical infrared study of the iron surface in aqueous sodium hydroxide [18]. In the first negative direction scan, there are two peaks before hydrogen evolution at −1.35 V vs SCE. The first peak at −1.1 V is due principally to the reduction of FeOOH to $Fe(OH)_2$, and the second one at around −1.3 V is due to the reduction of $Fe(OH)_2$ to iron metal. This first cathodic scan, however, is different from the first scan reported by Bewick *et al.* [18]. The peak seen at −1.1 V in Fig. 4 was not seen initially, but was seen in the later scans by Bewick *et al.* This probably means some Fe^{3+} species were present on the electrode surface when the first scan (shown in Fig. 4) was taken in the present study. Bewick *et al.* cathodically treated the iron by holding at −1.4 and then −1.2 V vs SCE, but no cathodic pretreatment was performed in the present study after the polishing of the electrode before Fig. 4 was recorded. The first scan in the positive direction shows only one prominent peak at −0.75 V vs SEC which has been attributed to the oxidation of Fe^{2+} oxide, $Fe(OH)_2$, to Fe^{3+} oxide, principally α-FeOOH as well as the δ and δ′ phases of FeOOH. $Fe(OH)_2$ formation from Fe metal is considered to begin at −1.0 V vs SCE, that is, at the foot of the wave peaking at approximately −0.75 V vs SCE. A small oxidation peak centered at about −1.12 V vs SCE corresponds to the formation of soluble dihypoferrite ($HFeO_2^-$) from oxidation of metallic iron [21, 22]. In spite of the formation of soluble species during the scans, the peaks for the reduction of insoluble Fe^{3+} oxide to insoluble Fe^{3+} oxide and the oxidation of insoluble Fe^{3+} oxide to insoluble Fe^{3+} oxide continued to become larger with potential cycling. This is consistent with visual observation of oxide buildup on the electrode surface after a number of potential scans. The peak for the oxidation of metallic iron to soluble Fe^{2+} oxide (i.e., dihypoferrite) at about −1.12 V vs SCE stayed the same in magnitude even after a number of potential cycles. At potentials more positive than the wave peaking at −0.75 V vs SCE, the steel is passivated, and only a small faradaic current flows until the potential is greater than +0.5 V vs SCE, which corresponds to onset of the oxidation of water form molecular oxygen.

Window opening experiments (not shown) indicate that in the negative going scan, the peaks at −1.1 V vs SCE for Fe^{3+} reduction and at −1.3 V for Fe^{2+} reduction are suppressed if the preceding positive going scan is reversed before reaching −0.8 V vs SCE, which is the potential at which the conversion of the passive layer oxides to the Fe^{3+} oxidation state is expected to occur. After the first scan (solid line in Fig. 4), the ratio between the peak height for the peak at −1.3 V and the peak at −1.1 V decreased. This indicates that the amount of $Fe(OH)_2$ being reduced to iron metal was less than amount of FeOOH being reduced to $Fe(OH)_2$, that is, the reduction of ferrous species to metal is not as great as the reduction of ferric species to ferrous species per cycle. This suggests that the kinetics for reduction of Fe^{2+} to metal is slower than the kinetics for the reduction of Fe^{3+} to Fe^{2+}. This is consistent with the accumulation of oxides on the

surface with cycling of the steel potential and in turn explains why in the tenth scan the peak heights are all absolutely higher than the peak heights found in the first scan (compare solid and dotted lines in Fig. 4). The accumulation of oxides with potential cycling can be followed by measuring the growth of the peaks for the oxidation of Fe^{2+} to Fe^{3+} at −0.75 V and for the reduction of Fe^{3+} to Fe^{2+} at −1.1 V after each successive cycle.

With the RRDE in anaerobic aqueous alkaline solution, the voltammetry of the steel disc and the gold ring electrodes showed virtually no dependence on the forced solution convection caused by rotating the RRDE between up to 3600 rpm. In alkaline solution the steel voltammogram shows the current response for the potential-induced valency changes of iron in the passive layer restricted to the electrode surface. As mentioned above, some dissolution of metallic iron or oxide iron is possible in the form of soluble dihypoferrite ($HFeO_2^-$) near the cathodic end of the scans [21, 22], but slow accumulation of oxides from metal oxidation was visually confirmed on the electrode surface.

Figure 5 shows the cyclic voltammogram of the steel disc in aqueous 1 M KOH solution under nitrogen (solid line) and oxygen (dotted line) atmosphere when the potential windows was made narrower by around 0.3 V on the cathodic side to −1.25 V vs SCE and by around 0.6 V on the anodic side to −0.05 V vs SCE. The negative direction scan in the voltammogram of steel under an inert atmosphere (solid line) shows oxide reduction ($Fe^{3+} \rightarrow Fe^{2+}$) beginning at about −0.65 V and peaking at −1.1 V vs SCE. The positive scan shows a peak corresponding to the reoxidation of the ferrous oxide at −0.8 V vs SCE. During the negative direction scan of the steel in the presence of O_2 (dotted line), the curve drops below the zero current line at about −0.4 V vs SCE and not −0.65 V as was found in an inert atmosphere. This early extra reduction current is due to oxygen reduction. At potentials more negative than −0.4 V, the dotted line is translated below the solid line in Fig. 5,

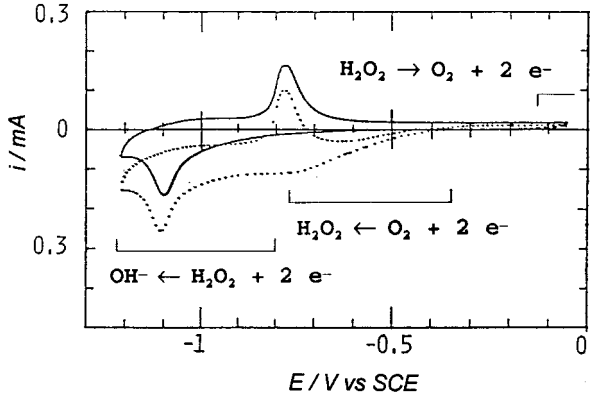

Fig. 5. Cyclic voltammogram of ASTM A516 steel disc (dia. 0.608 cm) in aqueous anaerobic 1 M KOH solution (pH 14). Scan rate 10 mV s^{-1}. Solid line: under N_2. Dotted line: equilibrated with 1 atm of O_2 over solution.

because the dotted line represents the sum of O_2 and oxide reduction, whereas the solid line is only for oxide reduction on steel. The peroxide oxidation is due to the peroxide that remained in the diffusion layer after it formed by oxygen reduction on steel during the preceding negative direction scan. This extra oxidation is hardly evident when diffusion is the only mass transfer mechanism, but is clearly noticeable in the presence of convection (*vide infra*).

The oxide layer thickens with each successive cycle, when the steel electrode in alkaline solution was cycled over a wide potential range, such as that discussed in Fig. 4 above. When the potential window was narrowed down by about 0.3 V on the cathodic side to −1.25 V vs SCE and by 0.6 V on the anodic side to −0.05 V vs SCE, the change in the amount of surface oxide per cycle was very small, and this is evident by a larger peak current (0.5 mA) in the voltammogram in Fig. 4 compared to the peak current (0.25 mA) in the voltammogram shown by the solid line in Fig. 5. This narrower range of potentials is suitable for measuring the oxygen reduction polarization curves, because there is no oxygen reduction at the anodic potential limit, −0.05 V vs SCE, and oxygen reduction is diffusion limited near the cathodic limit at about −1.2 V vs SCE (see dotted line Fig. 5). The freshly polished electrode was held at −1.4 V vs SCE, for about 10 min, and then cycled between −0.05 and −1.25 V vs SCE prior to and after oxygen (O_2) reduction experiments to check the state of the electrode/solution interface. Using this procedure, the voltammogram shown in Fig. 5 (solid line) was consistently reproduced during the O_2 reduction study. The peak heights were the same before and after the oxygen reduction measurements. This indicates the oxide coverage on the metal was essentially the same before and after the measurement.

The amount of oxide covering the metal can be estimated from the charge for a well-behaved valency change in the oxide film (e.g., in the steel voltammogram) integrating either the oxidation ($Fe^{2+} \rightarrow Fe^{3+}$) wave peaking at around −0.75 V vs SCE or reduction wave peaking at around −1.1 V vs SCE in the voltammogram shown in Fig. 5 gives a charge of about 5×10^{-4} C and indicates that the oxide coverage on the steel disc was about 5×10^{-9} mole per 0.3 cm^2 of steel electrode area. The volume of iron oxides like hematite can be approximated by a cube of 4 Å on a side. Thus, from the voltammogram shown in Fig. 5, about 5×10^{-9} moles of oxide found on the 0.3 cm^2 steel disc electrode indicates that approximately 15 to 20 minelayers, or about 60 to 80 Å, of oxide covered the steel disc electrode during the O_2 reduction measurements in 1 M KOH.

Figure 6 shows the cyclic voltammogram of gold in aqueous anaerobic borate buffer (pH 9.8) with and without the addition of hydrogen peroxide. The gold foil electrode was flame annealed and cycled once to remove chemically produced gold oxide from the electrode surface, and then the voltammogram was recorded as shown (Fig. 6, solid line). The borate

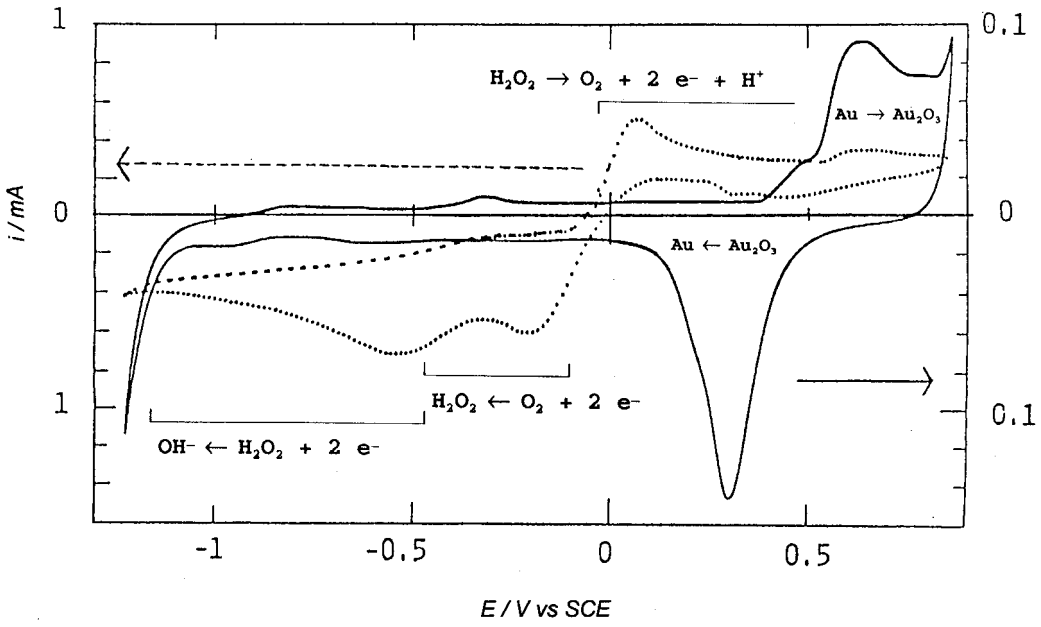

Fig. 6. Cyclic voltammogram of a gold electrode in aqueous anaerobic borate buffer (pH 9.8) solution without (solid line) and with (dotted line) 0.025 M hydrogen peroxide added. Scan rate 20 mV s^{-1}. Electrode area 2.5 cm^2.

buffer was lower in ionic strength than the aqueous 1 M KOH solution, so the scan rate is slower in borate to minimize the effects of increased solution resistance in the aqueous borate versus KOH solution. The major features observed in the first anodic scan (Fig. 6, solid line) are the gold oxide formation, which began at around +0.4 V vs SCE and continued through to the onset of O_2 evolution that occurred around +0.9 V vs SCE. The cathodic scan showed the reduction of the surface gold oxide peaking at around +0.35 V vs SCE and hydrogen evolution beginning at around −1.25 V vs SCE. Cycling was continued as the solution was stirred, and an aliquot of concentrated hydrogen peroxide was added to the aqueous borate solution resulting in an electrolyte solution with a final H_2O_2 concentration of 0.025 M. Stirring was stopped, and then the voltammogram was recorded beginning at 0 V vs SCE and scanning in the negative direction. The voltammogram of gold in the aqueous borate buffer solution with added H_2O_2 (Fig. 6, dotted line) was markedly different from that in aqueous borate buffer alone (Fig. 6, solid line). There was pronounced peroxide oxidation between −0.05 to +0.9 V vs SCE, and a reduction beginning at −0.05 V and continuing up to the cathodic limit at −1.25 V vs SCE. These peroxide faradaic currents were much larger than the currents for the gold surface processes in the absence of peroxide (note the tenfold change of scale for the current axes). In still solution, the faradaic currents diminished with successive scans (not shown), but if the solution was stirred briefly, the higher faradaic currents seen for the initial curve (shown by dotted line in Fig. 6) were restored.

Under cathodic protection, the pH of the water layers within a crevice near a holiday becomes mildly alkaline (e.g., 9), and under some extreme conditions, though unusual, the pH may be expected to become as high as 14. The voltammetry of steel was studied at a milder alkalinity using borate buffer (pH 9.8) as well as at pH 14, as discussed above. The results were essentially the same with borate buffer at pH 9.8 as in the stronger alkali (pH 14) discussed above, but with some retarding of oxide growth probably due either to greater dissolution of the oxide in the borate buffer (more acidic) limiting the oxide buildup, or alternatively to a relatively stronger adsorption of borate ion compared to hydroxide ion on steel, thereby suppressing the oxide formation. Further study, however, is needed to resolve the cause of the relatively thinner oxide film in borate buffer versus OH^- electrolytes. Figure 7 shows the voltammogram for the second scan of ASTM A516 steel in anaerobic aqueous borate buffer (pH 9.8) solution. The upper potential limit was −0.05 V vs SCE and the lower limit was −1.05 V vs SCE. The electrode was held at −1 V vs SCE for about 10 min and then scanned be-

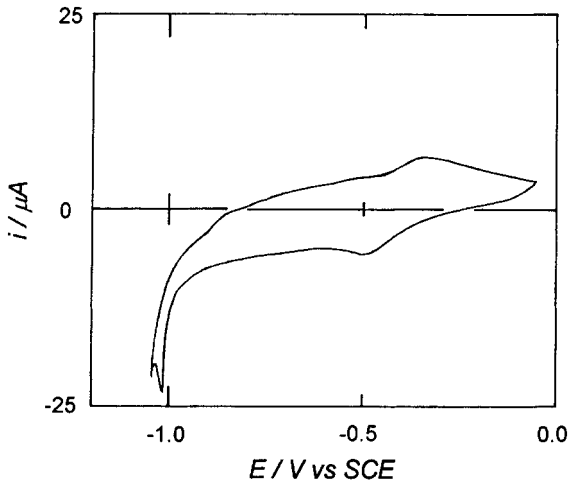

Fig. 7. Cyclic voltammogram of ASTM A516 steel disc (dia. 0.608 cm) in aqueous anaerobic borate buffer solution (pH 9.8). Scan rate 1 mV s^{-1}.

ginning in the negative direction. This voltammogram is very similar to that reported for pure iron in the same electrolyte solution [2]. The voltammogram persisted with no changes for many cycles. Eventually, after cycling for a few hours, the positive peak at around −0.25 V vs SCE and the negative peak at −0.45 V grew in height. This indicates that oxide was accumulating on the surface, but very slowly.

4.2. *Rotating ring disc electrode (RRDE) experiments*

4.2.1. Oxygen reduction in borate buffer (pH 9.8). Using the rotating steel disc with gold ring electrode, oxygen was reduced on an ASTM A516 steel disc (Fig. 8(a)) in aqueous borate buffer (pH 9.8) equilibrated with 1 atm of oxygen over solution, which resulted in the detection of significant amounts of peroxide at the gold ring (Fig. 8(b)). In Fig. 8, the solid lines represent the current measured during the negative direction scan of the disc, and the dotted lines represent the current measured during the positive direction scan of the disc. No peroxide oxidation current was detected at the gold ring when the experiment was conducted with the electrolyte equilibrated with 1 atm of N_2 instead of O_2 over solution. Peroxide was detected by measuring the peroxide oxidation current on the gold ring at +0.4 V vs SCE. At this ring potential, peroxide oxidation is mass-transport limited (see discussion of Fig. 6 above). Oxygen reduction on steel began at about −0.1 V vs SCE and continued down to the hydrogen evolution region, that is, −1.1 V vs SCE. Peroxide generation was detected between −0.1 and −0.7 V vs SCE, and the maximum rate of peroxide generation occurred between −0.3 and −0.4 V vs SCE; for example, when the electrode was rotated at 400 rpm, the maximum amount of peroxide current found on the gold ring occurred when the disc potential was approximately −0.4 V vs SCE. The measured current for peroxide oxidation on the gold ring was 0.048 mA, and when this current was corrected for collection efficiency of the gold ring, the actual peroxide oxidation current was determined to be approximately 58% of the oxygen reduction current on the steel (0.36 mA). At more negative potentials (−0.6 to −1.1 V vs SCE), O_2 reduction yielded the four-electron reduction product, water (OH^- in alkaline media) and essentially no two-electron reduction product, peroxide. The current for peroxide oxidation on the gold ring approaches zero in this potential range (see Fig. 8(b) in the region −0.6 to −1.1 V vs SCE).

When the disc potential was scanned in the positive as opposed to negative direction, there was a small but noticeable hysteresis for O_2 reduction current on the steel disc as well as for the H_2O_2 oxidation current on the gold ring set a +0.4 V vs SCE (see Fig. 9(a) and (b)). At a particular potential, the current for O_2 reduction on steel is slightly greater when the potential is approached by scanning in the positive direction, and as a result the curve for the oxygen reduction on steel is slightly shifted to positive potentials when comparing scans taken in the positive compared to negative direction (see Fig. 9(a)). This scan direction dependent hysteresis can be accounted for by considering that the steel electrode surface is more active toward oxygen reduction when it is in the more reduction versus more oxidized state. For any particular potential, the electrode would be more reduced when that potential is approached by a scan proceeding toward the positive direction than by a scan proceeding toward the negative direction.

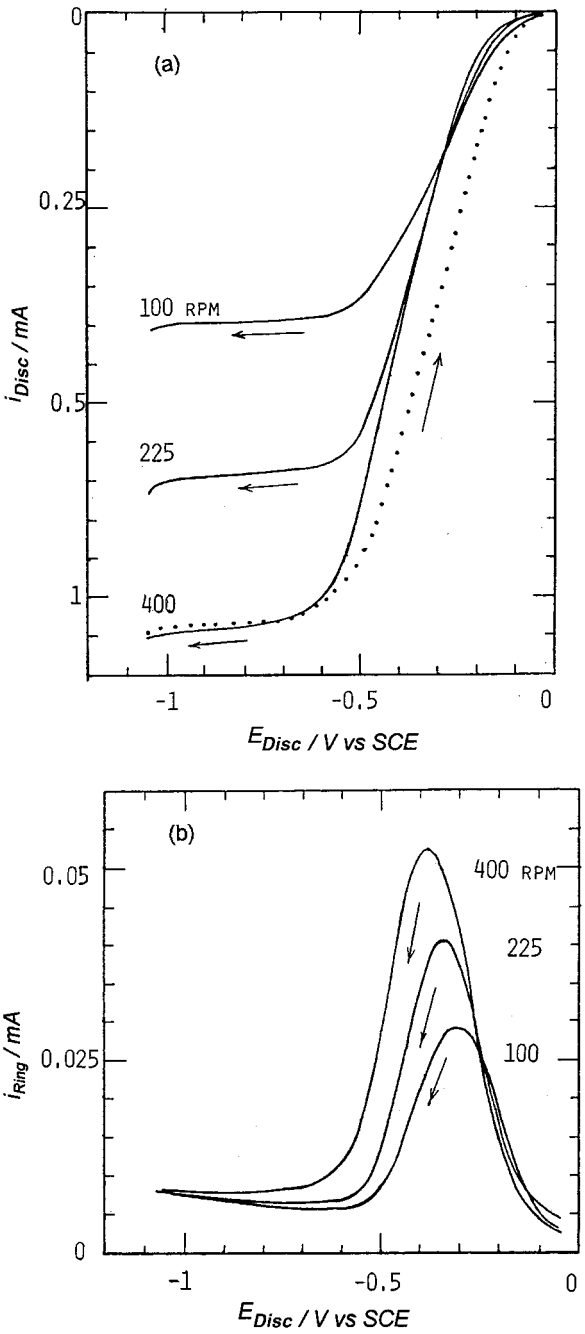

Fig. 8. (a) Quasi-steady state polarization curve for ASTM A516 steel disc (dia. 0.608 cm) in aqueous anaerobic borate buffer (pH 9.8; 0.02 M sodium borate, 0.023 M KOH) equilibrated with 1 atm of oxygen over solution. Scan rate 1 mV s^{-1}. Solid lines for negative direction and dotted line for positive direction scans. (b) Gold ring (i.d. 0.75 cm, o.d. 0.85 cm) current for the oxidation of the disc product, peroxide. Ring potential +0.4 V vs SCE. Collection efficiency, $N = 0.24$. Rotation rates 100, 225 and 400 rpm. Solid lines for negative direction scans.

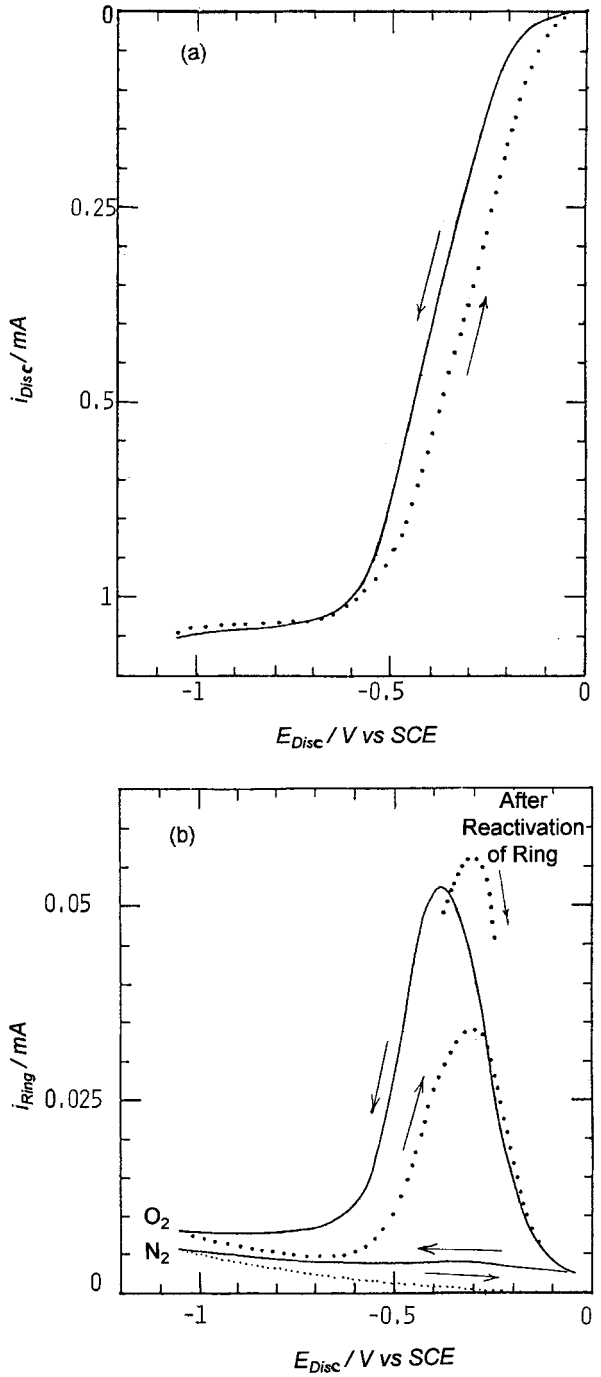

Fig. 9. (a) Quasi-steady state polarization curve showing effect of scan direction for O_2 reduction on ASTM A516 steel disc (dia. 0.608 cm) in aqueous borate buffer solution (pH 9.8) equilibrated with 1 atm of oxygen over solution. Scan rate 1 mV s^{-1}. (b) Gold ring (i.d. 0.75 cm, o.d. 0.85 cm) current for the oxidation of the disc product, peroxide. Ring potential +0.4 V vs SCE. Collection efficiency, $N = 0.24$. Solid lines for negative direction and dotted line for positive direction scans. Rotation rate 400 rpm.

Hysteresis for the peroxide oxidation current at the gold ring paralleled the hysteresis found on the steel disc (see Fig. 9(b); solid lines for negative scan direction and the top dotted lines for the positive scan direction). A slightly larger peroxide oxidation current was found on the gold ring during the positive direction scan, and this reflects the slightly larger oxygen reduction current found on the steel disc at any given potential during the positive direction scan compared to the negative direction scan. There was no indication of a change in the O_2 reduction mechanism as a result of scan direction. Under some conditions, a greater hysteresis was observed by this work and reported by others [2] for the peroxide oxidation on the gold ring with scan direction of the disc potential, but this greater hysteresis apparently was an artifact and most likely due to the effects of trace impurities in solution (see Fig. 9(b) the solid versus the dotted lines). The rationale is as follows. The ring was activated by cycling its potential through the gold oxide formation and reduction region. The gold ring potential was then set at +0.4 V vs SCE. The experiment was begun by scanning the steel disc in the negative direction accompanied by detection of peroxide at the gold ring. When the negative scan limit, −1.2 V vs SCE, was reached, the scan direction of the disc was immediately reversed toward the positive direction with no reactivation of the gold ring by a potential cycling treatment. The ring current for this anodic scan was about two thirds of that measured on the preceding cathodic scan (see Fig. 9(b); the solid versus the dotted lines). A different result is found, on the other hand, if the gold ring was reactivated by cycling it, and then setting it at the peroxide oxidation potential, +0.4 V vs SCE, just before and without interrupting the anodic scanning of the disc. With reactivation of the gold ring, the ring current for H_2O_2 oxidation during the anodic scan of the disc potential rose to levels comparable to those measured during the cathodic scan (see Fig. 9(b); compare the top solid line and the top dotted line). There was a slight enhancement for the positive scan due to increased activity of the disc at a given potential, as discussed above. For the positive scan direction, with the electrode rotated at 400 rpm, the maximum peroxide generation current, 0.24 mA (corrected for collection efficiency), was found when the disc potential was around −0.31 V vs SCE with a disc current of 0.4 mA. This corresponds to 60% of the O_2 reduction current at −0.31 V giving rise to peroxide generation.

4.2.2. Oxygen reduction 1 M KOH (pH 14). The same ring-disc electrode was polarized in aqueous 1 M KOH (pH 14) equilibrated with 1 atm of oxygen over solution, so that O_2 was reduced on the ASTM A516 steel disc (Fig. 10(a)), and this gave rise to peroxide oxidation current on the gold ring (Fig. 10(b)). In 1 M KOH, the potential of the peroxide detecting gold ring electrode was set at +0.05 V vs SCE, a potential at which peroxide oxidation is mass transport limited (Fig. 3). Figure 8 shows the negative direction potential scan of the steel electrode in the presence of oxygen as the electrode was rotated at 100, 400, 1600 and 3600 rpm. Oxygen reduction on steel began at about −0.2 V vs SCE and continued up to the hydrogen evolution region, that is, just more negative than −1.2 V vs SCE. The inflection in the curve found at about 0.6 V is discussed below. Peroxide was generated between −0.2 to −0.9 V vs SCE. The maximum rate of peroxide generation, which was found to be

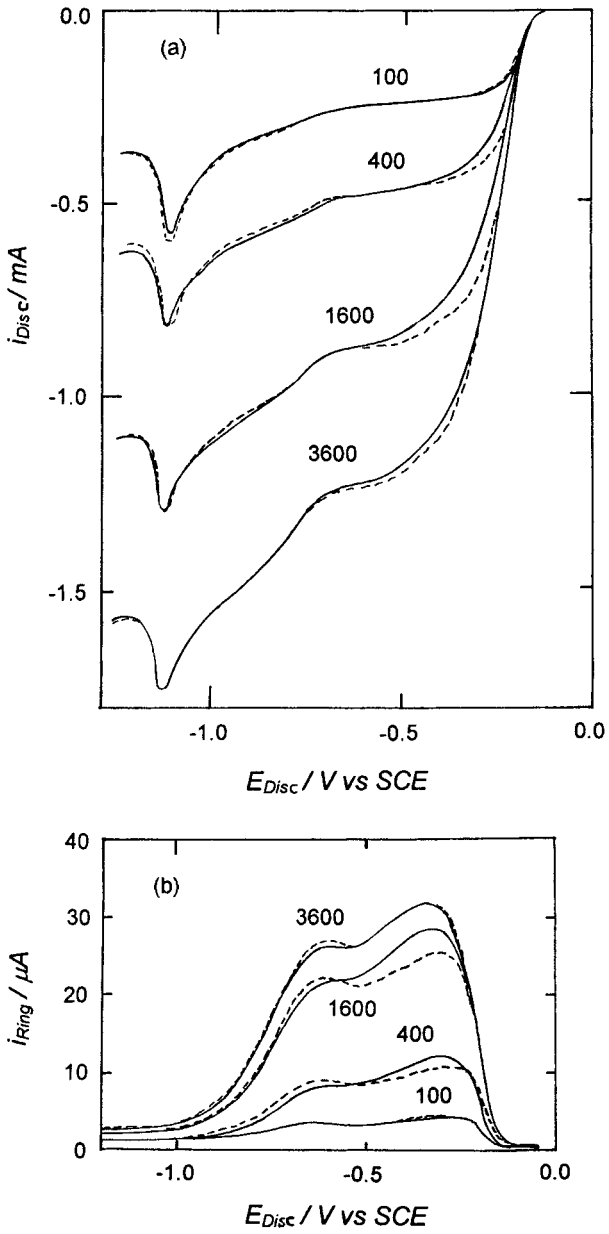

Fig. 10. (a) Quasi-steady state polarization curve for O_2 reduction on ASTM A516 steel disc (dia. 0.608 cm) in aqueous 1 M KOH solution (pH 14) equilibrated with 1 atm of oxygen over solution. Scan rate 10 mV s^{-1}. (b) Gold ring (i.d. 0.75 cm, o.d 0.85 cm) current for the oxidation of the disc product, peroxide. Ring potential +0.05 V vs SCE. Collection efficiency, $N = 0.24$. Rotation rates 100, 400, 1600 and 3600 rpm.

about 10% of the oxygen reduction current, and this level of peroxide was detected by the ring when the disc potential was between −0.3 and −0.7 V vs SCE. During these oxygen reduction studies in 1 M KOH, the disc was only scanned in the negative direction. The dotted line is for a replicate run performed immediately after the run represented by the solid line.

The peroxide oxidation current on gold was only observed when dissolved O_2 was reduced on the steel electrode in the KOH electrolyte, and was not found when the electrolyte was equilibrated with a N_2 atmosphere over solution. The solution was alternately equilibrated with O_2 then N_2 several times, and the oxidation current on gold appeared every time the steel disc potential was scanned to oxygen reduction potential with O_2 in solution and disappeared every time the O_2 was purged out by N_2.

The peroxide oxidation current detected at the ring exhibited a local minimum at about −0.6 V vs SCE (see Fig. 10(b)). Three possible explanations are: (i) a reduction of iron as well as O_2 on the disc electrode resulting in a lowering of the oxygen reduction current and leading to proportionately lower peroxide generation; (ii) formation of disc reduction products that catalyse decomposition of peroxide lowering the peroxide arriving at the ring; or (iii) the passive layer on the steel disc may form reduction products that dissolve and adsorb on gold and foul the gold ring's peroxide detection capability. Reduction of the iron oxide on the electrode surface begins at around −0.6 V vs SCE (see Figs 4 and 5). At around −0.6 V, the disc current may be a mixed current with some disc current going for the reduction of small amounts of iron oxide in the passive layer leading to diminished O_2 reduction on the steel disc. This would consequently yield a proportionately diminished peroxide oxidation on gold, and hence possibly explaining the two maxim for peroxide oxidation at the gold ring centred about −0.6 V vs SCE. Catalytic decomposition of peroxide by the action of ferrous species is a possibility, but why this would be maximal at −0.6 V vs SCE is not clear. The presence of adventitious impurities desorbing from steel and masking or deactivating the gold electrode could be the most likely cause of the two maxima. Two maxima were not always observed, instead a single maximum at about −0.7 V was seen sometimes during the present investigation. Work to resolve this issue is in progress. At more negative potentials (−0.85 to −1.25 V vs SCE), O_2 reduction yielded mostly the four-electron product, water (OH^- in alkaline media) since essentially no two-electron product, peroxide, was detected on the gold ring electrode. The faradaic current for peroxide oxidation on the gold ring approaches zero in this potential range (see Fig. 9(b) in the region −0.85 to −1.25 V vs SCE).

Assuming that there is greater catalytic activity of the metallic surface compared to the oxide covered surface for the four-electron reduction of O_2 to water, it is reasonable to rationalize that the shifting of the O_2 electroreduction product from peroxide to water is due to the formation of metallic iron on the surface at potentials negative of −0.85 V vs SCE. Anaerobic steel voltammetry (see discussion for Figs 4 and 5 above) as well as spectroelectrochemical FTIR studies of iron in 1 M alkaline solution [19] indicate, however, that iron metal oxidizes to ferrous oxide as early as −1.15 V vs SCE and the electroreductive conversion of iron oxide to metallic iron is not expected until about −1.3 V vs SCE, but even at −1.3 V the oxide may not completely be removed from the surface of the electrodes. At potentials more negative than −0.85 V vs SCE, it is difficult to determine if the four-electron product is the favored product of O_2 electroreduction on a reduced iron oxide surface via a series mechanism, or if small amounts of metallic iron

remains on the surface at these potentials and dominates the kinetics via a direct four-electron pathway. Direct four-electron reduction of O_2 on an iron oxide surface is also a possibility at high overpotentials (−0.85 to −1.25). Although it is possible that at high overpotentials (−0.85 to −1.25), the direct four-electron reduction of O_2 may occur on a steel electrode with the surface containing iron metal patches or with the surface being completely covered with iron oxide, these situations seem unlikely. The most likely pathway for hydroxide formation at high overpotentials (−0.85 to −1.25), is via a series mechanism on a reduced iron oxide surface.

Support for the series path, involving the reduction of oxygen to peroxide and then peroxide to hydroxide at high overpotentials is given in Fig. 11. The dotted line in Fig. 11 is the polarization curve for the ASTM A516 disc rotated at 1600 rpm in 1 M aqueous KOH solution with added peroxide in an inert (N_2) atmosphere. The peroxide was introduced by adding a small aliquot of 50% aqueous peroxide solution to the degassed 1 M KOH electrolyte. The peroxide concentration was made 1 mM, the same concentration as for O_2 dissolved in dilute aqueous alkaline electrolyte when it is equilibrated with 1 atm of O_2 gas over solution [23, 24]. Peroxide reduction on steel is hardly evident when the anaerobic 1 M KOH plus 1 mM H_2O_2 solution was quiescent (see Fig. 11 solid line), but at 1600 rpm, a clear wave for peroxide reduction was observed between around −0.6 to −1.2 V vs SCE (Fig. 11, dotted line). Although it is not readily evident in the curve shown in Fig. 11, a small H_2O_2 oxidation current, which began at −0.15 V vs SCE and which was rotation-dependent, was sometimes noticeable, particularly after the electrode had been cycled many times between −0.05 and −1.2 V vs SCE. The portion of the curve between −0.6 and −1.2 V for peroxide reduction on the steel disc rotated at 1600 rpm appears to be essentially the same as the

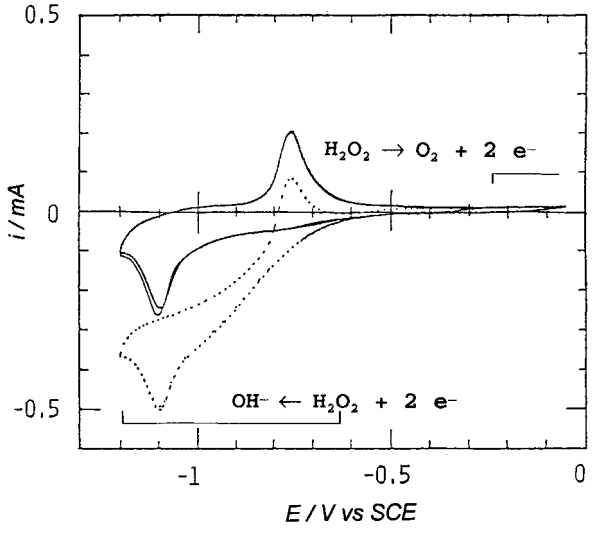

Fig. 11. Cyclic voltammogram of ASTM A516 disc (dia. 0.608 cm^2) in 1 M KOH with 1 mM H_2O_2 under a N_2 atmosphere. Solid line: no convection of solution. Dotted line: disk rotated at 1600 rpm. Scan rate 10 mV s^{-1}.

second half of the curve for O_2 reduction on the same steel disc in KOH solution equilibrated with 1 atm of O_2 over solution (see Fig. 10(a) at 1600 rpm). In Fig. 10(a), the first wave in the curve for the oxygen reduction on steel between −0.2 to −0.6 V vs SCE is probably due to the reduction of O_2 to H_2O_2, which plateaus at −0.6 V. This first reduction step continues at more negative potentials. This establishes the baseline to which is added the current for the reduction of H_2O_2 to OH^- which occurs between −0.6 to −1.2 V vs SCE (Fig. 10(a)). The second wave of the curve in Fig. 10(a) is a virtually identical to the peroxide reduction curve found between −0.6 to −1.2 V shown in Fig. 11, and this suggests that O_2 reduction on steel in basic solution proceeds by two sequential two-electron reductions.

Electrooxidation of peroxide on steel in 1 M KOH occurs at about −0.2 V vs SCE and more positive potentials, as observed in the polarization curve in Fig. 11 (peroxide oxidation on steel in 1 mM peroxide in 1 M KOH under N_2 with the rotation rate at 1600 rpm). This observation evokes a rationalization for explaining why the onset of current for O_2 reduction in 1 M KOH was delayed until −0.2 V vs SCE instead of being seen at −0.07 V vs SCE as expected from thermodynamics (see Table 1). The cathodic current for O_2 being reduced to peroxide was probably offset by an anodic current for the newly formed peroxide being oxidized back to O_2, so no net current results for the negative going scan up to −0.2 V vs SCE. For potentials more negative than −0.2 V vs SCE, the oxidation of the peroxide is no longer expected to occur on steel in 1 M KOH (Fig. 11), so only O_2 reduction on steel occurred and a net negative current was seen starting at this point in the scan (Fig. 9). These observations support the series mechanism for oxygen reduction on steel in 1 M KOH; that is, a series of two two-electron reduction steps, with the first step at low overpotentials being the two-electron reduction of O_2 to peroxide.

During the O_2 reduction on the steel disc in 1 M KOH solution between −0.2 to −0.6 V vs SCE, the peroxide oxidation current on the gold ring did not show that 100% of the O_2 reduced on steel in this potential region was going to peroxide generation. Instead, it appeared that only around 10% of the O_2 reduced gave rise to peroxide generation. This discrepancy is likely due to inhibition of the gold ring to peroxide oxidation due to trace impurities in the solution. The gold ring was intermittently reactivated by cycling and then set at +0.05 V vs SCE during the uninterrupted sweeping of the steel disc in 1 M KOH with 1 atm O_2 over solution. In this experiment, only one peak was observed (not shown) for the H_2O_2 oxidation on the gold ring. This one peak for the H_2O_2 oxidation current on the gold ring was found when the disc potential was around −0.7 V vs SCE, and the peak current (corrected for collection efficiency) for peroxide oxidation on the gold ring was not 10% but was about 50 to 60% of the O_2 reduction current on the steel. Although this experiment qualitatively

showed that much more than 10% of the O_2 electroreduction yielded peroxide generation as expected based on the results from Fig. 10, it was difficult to consistently and completely activate the gold ring toward H_2O_2 oxidation by the intermittent cycling of the gold ring potential. A better way to avoid uncertainty in the results due to gold ring deactivation is to obtain the O_2 reduction and H_2O_2 oxidation currents by using a different RRDE method, namely, the cyclic potential ring measurement (CPRM) method [19]. The CPRM technique involves holding the steel disc at a fixed O_2 reducing potential and recording the steady state voltammogram of the gold ring rapidly cycling through the gold oxide formation and reduction regions. In this situation, the gold ring oxidizes peroxide as it is continually being reactivated by the cycling. This requires further consideration and is the subject of ongoing work.

5. Discussion

The voltammetry of ASTM A516 steel performed in alkaline solutions showed that the surface of this steel is similar to pure iron [2, 18] and low carbon steel [3, 13]. The surface oxides were found to form at potentials just positive of hydrogen gas evolution on steel (−1.15 V vs SCE in 1 M KOH). Although holding the steel surface in the H_2 evolution region could remove the oxide that remained after exposing freshly polished steel to air, once an appreciable amount of oxide formed on the surface, it persisted even if the potential were held in the hydrogen evolution region for several minutes. This suggests that the O_2 electroreduction on steel is, for practical purposes, occurring on an oxide surface in virtually all cases.

The RRDE technique employing a steel disc and gold ring was useful for learning about the O_2 reduction products on steel. As O_2 was reduced on the steel disc, peroxide was detected by the gold ring over a wide potential range. The peroxide detection, and subsequently the insight into the O_2 reduction mechanism, is considered qualitative after this study, mainly because trace impurities in solution deactivated the gold ring to some degree and prohibited the quantitative detection of peroxide. This prevented the numerical evaluation of the rate constants needed to rigorously deduce the mechanism. Nevertheless, the RRDE measurement showed that the most likely pathway for O_2 reduction on iron-based electrodes is via the series mechanism, that is, by two sequential two-electron steps. Thus, the direct four-electron reduction of O_2 is not catalysed on steel, so k_1 is small. Therefore, peroxide formation is expected to occur on the surface of steel pipes under cathodic protection conditions, since O_2 reduction on steel in alkaline media proceeds via a two sequential two-electron steps. This mechanism appears likely over the entire range of potentials from the onset of O_2 reduction down to water reduction. At potentials as far negative as about −0.7 V vs SCE for oxygen reduction on steel in 1 M KOH, peroxide generation is expected to be the dominant process, because k_2 is expected to be larger than either k_1 or k_3. Some peroxide generation and liberation into solution may persist even as negative as −0.9 V vs SCE. This dominance of peroxide generation at lower overpotentials, consistent with the series mechanism, is supported by the data in Table 3, where the O_2 reduction process on steel is shown to yield mainly peroxide at low overpotentials. At potentials more negative than −0.7 V vs SCE in 1 M KOH, k_3 is expected to become larger than k_2, and the second step (the reduction of peroxide) causes the O_2 reduction process to yield mainly hydroxide in solution at highly negative potentials. This explains the drop off in the peroxide detection by the gold ring at highly negative potentials. Most of the peroxide is being further reduced to hydroxide on the steel disc, instead of being released into solution and to the gold ring where it can be detected as oxidation current. At more negative potentials (more negative than −1.2 V vs SCE in 1 M KOH), water as well as oxygen reduction occurs at more negative potentials. The products of water reduction are molecular hydrogen and hydroxide. Hydrogen may be even more damaging than peroxide to the adhesion of protective coatings on steel, and this region should be avoided when cathodically protecting coated steel pipelines.

Oxygen reduction as well as peroxide oxidation and reduction involve protons, and the formal potentials for these processes are expected to shift $\sim$59 mV decade^{-1} of pH. Accordingly, the peroxide producing potential range is expected to be more shifted to positive potentials in less basic solutions (e.g., peroxide production peaking at about −0.4 V vs SCE and not found more negative than −0.7 V vs SCE in the borate buffer (pH 9.8); but peaking at about −0.7 V, and found as negative as −1 V in the OH^- electrolyte (pH 14) studied here), but the

Table 3. Percentage of O_2 reduction current going to peroxide generation

Solution	*Scan direction*	*Rotation rate*/rpm	*Potential*/V vs SCE	% *Peroxide**
Borate	−	400	−0.4	58
Borate	+	400	−0.31	60
Borate	−	225	−0.35	52
Borate	−	100	−0.32	42
KOH	−	1600	−0.6 (−0.7†)	10 (50†)

* Fraction, F, O_2 current making H_2O_2 = (Ring current × 1/N)/(Disc current) where N (collection efficiency) = 0.24. % Peroxide = 100 F. † With intermittent reactivation of gold ring.

mechanism of O_2 reduction is probably the same, that is, the series mechanism. The shift in O_2 reduction potential by pH shift is consistent with the results of the RRDE studies for O_2 reduction and peroxide generation on steel in borate buffer and potassium hydroxide electrolytes equilibrated with 1 atm of O_2 over solution are summarized in Table 3. The pH of the ground water adjacent to the protected steel surface will rapidly become strongly alkaline due to hydroxide generation from either O_2 or water reduction, and this will drive the cathodically protected steel surface into the range of conditions for producing peroxide.

Electrochemically generated peroxide can have adverse effects on a protective organic coating mainly for two reasons. First, peroxide generation can occur at the boundary between the coating and the steel near a holiday or even beneath intact coatings [25]. This is precisely where the peroxide and its decomposition products can do the greatest harm, because chemical attack at the interfacial region can lead to delamination of the organic coatings. The delamination front would be expected to start a holiday and grows radially outward with a thin film of aqueous electrolyte collecting between the steel surface and an intact overlayer of polymer. The steel surface within the holiday and under the thin film of electrolyte become susceptible to corrosion when the cathodic protection is inadequate, and the electrical power needed to maintain satisfactory level of cathodic protection may increase according. Secondly, even if most of the peroxide were to form on the bare steel surface of the holiday far from the interface between the steel and polymer, the peroxide, which is believed to be strongly adsorbed on the steel [3], may rapidly migrate to the polymer/metal interface by surface diffusion over the steel surface. As peroxide is consumed during its chemical attack on the polymer, a surface concentration gradient will form, and this gradient will drive the peroxide from the centre of the holiday surface out toward the edge of the holiday surface where the polymer is found. Further, as peroxide builds up on the iron surface, it may be converted to harmful superoxide and hydroxy radical species as shown in Table 2. The nature of the role of peroxide and its related species to damage of coatings and interfacial compounds is the subject of ongoing work.

6. Conclusion

Peroxide was found to be generated during the reduction of O_2 on steel in aerobic aqueous alkaline solutions. Two sequential two-electron reduction steps (i.e., a series mechanism: first a two-electron reduction to peroxide, followed by another two-electron reduction of the peroxide to hydroxide) appears to be the likely pathway for O_2 reduction under the conditions studied. The conditions that peroxide was found to be generated are particularly relevant to the cathodic protection of steel. Therefore, schemes involving the cathodic protection of steel using polymer coatings and cathodic polarization to minimize steel corrosion, should consider the effects of peroxide, since typical polymer coatings such as fusion bonded epoxy are known to be susceptible to degradation by oxidizing agents.

Acknowledgements

The authors thank Prof. Ernest Yeager of the Chemistry Department, Case Western Reserve University, and Dr K. Krist, Basic Research Group of the Gas Research Institute (GRI) for helpful discussions. This work was supported by GRI (contract: 5091-260-2110).

References

[1] V. Jovancicevic and J. Bockris, *J. Electrochem. Soc.* **9** (1986) 1797.
[2] S. Zecevic, D. Drazic and S. Gojkovic, *J. Electroanal. Chem.* **265** (1989) 179.
[3] H. Wroblowa and S. Qaderi *ibid.* **279** (1990) 231.
[4] H. Leidheiser and W. Wang, *J. Coatings Technol.* **53** 672 (1981) 77.
[5] J. H. Payer, B. Trautman and D. Gervasio, *in* Proceedings of CORROSION'93, Paper 579 (1993).
[6] W. Latimer, 'Oxidation Potentials', Prentice Hall, New York (1938), chapter 4.
[7] E. Yeager, *Electrochim. Acta* **29** (1984) 1527; E. Yeager, *Prog. in Batteries and Solar Cells* **3** (1980) 238.
[8] M. Tarasevich, A. Sadkowski and E. Yeager, 'Oxygen Electrochemistry', *in* 'Comprehensive Treatise of Electrochemistry', Vol. 6, (edited by B. Conway, J. Bockris, E. Yeager and R. White), Plenum Press (1984).
[9] C. Mortimer, 'Chemistry a Conceptual Approach', 2nd edn, Van Nostrand Reinhold Co., New York (1971), pp. 128–9.
[10] J. R. Churchill, *Trans. Electrochem. Soc.* **76** (1939) 341.
[11] P. Delahay, *J. Electrochem. Soc.* **97** (1950) 205.
[12] S. A. Olszowka, M. A. Manning and A. Barkatt, *Corrosion* **48** (1992) 411.
[13] D. Gervasio and J. H. Payer, "Paper presented at the Spring Meeting of the Electrochemical Society", St. Louis, MI, Extended Abstract 92-2 (1992) 56.
[14] W. Barb, J. Baxendale, P. George and K. Hargrave, *Trans. Faraday Soc.* **47** (1951) 462.
[15] R. C. Weast (Ed.), 'Handbook of Chemistry and Physics', 55th edn, CRC Press, Cleveland, OH (1984).
[16] W. Albery and S. Bruckenstein, *Trans. Faraday Sac.* **28** (1966) 1920.
[17] J. Ritter and J. Kruger, *Surf. Sci.* **96** (1980) 364.
[18] A. Bewick, M. Kalaji and G. Larramona, *J. Electroanal. Chem.* **318** (1991) 207. H. Neugebauer, A. Moser, P. Strecha and A. Neckel, *J. Electrochem. Soc.* **137** (1990) 1475.
[19] N. Vilambi and E. Taylor, *J. Electroanal. Chem.* **270** (1989) 61.
[20] R. Zurilla, R. Sen and E. Yeager, *J. Electrochem. Soc.* **125** (1978) 1103.
[21] M. Pourbaix, 'Atlas of Electrochemical Equilibria in Aqueous Solutions', Cebelcor, Brussels (1974).
[22] I. Song, D. Gervasio and J. H. Payer, *J. Appl. Electrochem.* **26** (1996) 1045.
[23] K. Gubbins and R. Walker, *J. Electrochem. Soc.* **112** (1965) 469.
[24] A. Yatskovskii and N. Fedotov, *Elecktrokhimiya* **5** (1969) 1052.
[25] J. Parks and H. Leidheiser, *Ind. Eng. Chem. Prod. Res. Dev.* **25** (1986) 1.